JOURNAL OF GEOPHYSICAL RESEARCH, VOL. 113, D23202, doi:10.1029/2007JD009742, 2008

Click Here for Full Article

Altitude effect in UV radiation during the Evaluation of the Effects of Elevation and Aerosols on the Ultraviolet Radiation 2002 (VELETA-2002) field campaign

Y. Sola,[1] J. Lorente,[1] E. Campmany,[1] X. de Cabo,[1] J. Bech,[1] A. Redaño,[1] J. A. Martínez-Lozano,[2] M. P. Utrillas,[2] L. Alados-Arboledas,[3] F. J. Olmo,[3] J. P. Díaz,[4] F. J. Expósito,[4] V. Cachorro,[5] M. Sorribas,[5] A. Labajo,[6] J. M. Vilaplana,[7] A. M. Silva,[8] and J. Badosa[9]

Received 20 December 2007; revised 21 July 2008; accepted 4 September 2008; published 5 December 2008.

[1] The Evaluation of the Effects of Elevation and Aerosols on the Ultraviolet Radiation 2002 (VELETA-2002) field campaign was designed to study the influence of aerosols and altitude on solar UV irradiance. The altitude effect (AE) was evaluated for UV irradiance under cloudless conditions by taking spectral and broadband measurements in SE Spain in the summer of 2002 at three nearby sites located at different heights (680 m, 2200 m, and 3398 m). A spectral radiative transfer model (Santa Barbara DISORT Atmospheric Radiative Transfer (SBDART)) was also applied, mainly to evaluate the tropospheric ozone impact on AE. Results are related to the optical properties and air mass origin of the aerosols as determined by back-trajectory analysis. During the 1-week observing period of the campaign, there were two main synoptic situations with different air masses (polar maritime and tropical continental air mass associated with a Saharan dust event). The AE showed a high dependency on wavelength, solar zenith angle, and aerosols, although the growth of the mixing layer during the day also caused substantial AE variability. Saharan dust caused an increase in AE, especially in the UVB region and in the erythemal irradiance. In the UVA (320–400 nm) band the AE ranged 6–8% km^{-1} at noon, while for the UVB (280–320 nm) band it reached 7–11% km^{-1}. The AE for erythemally weighted irradiance ranged from 11 to 14% km^{-1} between the lowest and highest stations when it was calculated from spectral measurements.

Citation: Sola, Y., et al. (2008), Altitude effect in UV radiation during the Evaluation of the Effects of Elevation and Aerosols on the Ultraviolet Radiation 2002 (VELETA-2002) field campaign, *J. Geophys. Res.*, *113*, D23202, doi:10.1029/2007JD009742.

1. Introduction

[2] Solar UV radiation plays an important role in biological processes that affect humans, animals and plants. Since the discovery of the Antarctic ozone layer depletion [*Farman et al.*, 1985], and the potential increase in the UV radiation level at the Earth's surface, considerable efforts have been made to improve instrumental UV networks and radiative transfer models used in forecasting UV radiation [*Bais et al.*, 2007] or in comparing ground observations with satellite retrievals (see among others *Krotkov et al.*, 1998, 2005; *Wetzel and Slusser*, 2005). Under cloudless conditions, the UV irradiance reaching the ground depends on a number of factors including solar zenith angle (SZA), total ozone column, surface albedo, turbidity of the atmosphere, and altitude. The study presented here is focused on the altitude effect (AE) on UV radiation. Global (i.e., diffuse plus direct) surface UV irradiance increases with altitude due to the shorter path length of the solar beam through the atmosphere and the consequent decrease of scattering and absorption. Each of these processes has its own spectral dependence, resulting in a characteristic spectral AE.

[1]Departament d'Astronomia i Meteorologia, Universitat de Barcelona, Barcelona, Spain.
[2]Grupo de Radiación Solar, Departamento Físicade la Tierra i Termodinámica, Universitat de València, Burjassot, Spain.
[3]Departamento de Física Aplicada, Facultad de Ciencias, Universidad de Granada, Granada, Spain.
[4]Departamento de Física, Facultad de Ciencias, Universidad de La Laguna, La Laguna, Spain.
[5]Grupo de Óptica Atmosférica, Facultad de Ciencias, Universidad de Valladolid, Valladolid, Spain.
[6]Agencia Estatal de Meteorología, Madrid, Spain.
[7]Departamento de Observación de la Tierra, Teledetección y Atmósfera, Estación de Sondeos Atmosféricos de El Arenosillo, INTA, Huelva, Spain.
[8]Centro de Geofisica de Évora, University of Évora, Evora, Portugal.
[9]Grup de Física Ambiental, Departamento de Física, Escola Politècnica Superior, Universitat de Girona, Girona, Spain.

Copyright 2008 by the American Geophysical Union.
0148-0227/08/2007JD009742$09.00

[3] Experimentally AE is expressed as the relative irradiance increase (in % km^{-1}) from the lower to the higher site [*Blumthaler et al.*, 1997; *Pfeifer et al.*, 2006]:

$$AE = \left(\frac{E_h - E_l}{E_l}\right) \cdot \frac{1}{z_h - z_l} \cdot 100, \quad (1)$$

where E_h and E_l are the irradiances at the higher and lower positions respectively, and $z_h - z_l$ is the difference in altitude between the sites in kilometers. Precisely, AE should be expressed in terms of pressure difference instead of altitude difference. This is physically consistent with the fact that the air mass contained in a given air layer between two pressure levels is approximately constant. More specifically, using radiative transfer modeling, *Krotkov et al.* [1998] demonstrated that percent UV change is linear with the pressure difference between two levels. However, in field studies the AE is usually defined in terms of altitude difference between fixed locations, neglecting small pressure corrections, so we followed this approach to perform comparisons with other studies.

[4] The choice of the irradiance band allows us to discriminate the behavior of the spectral AE or take an integrated value over a specific range, UVA (320–400 nm) or UVB (280–320 nm) for example. Moreover, in most applications, the UV AE is defined as the increase in the biologically effective irradiance with altitude. Overexposure to UV radiation has a large number of negative effects on humans. One of the most evident is erythema, which is strongly dependent on wavelength. Increasing awareness of these harmful effects had led to the use of the biologically effective irradiance (with the appropriate action spectrum). Equation (2) describes the erythemally weighted irradiance, E_{er},

$$E_{er} = \int_{280}^{400} E_\lambda \cdot \varepsilon_\lambda d_\lambda, \quad (2)$$

where $E\lambda$ is the spectral irradiance and $\varepsilon\lambda$ is the erythemal action spectrum according to the International Commission on Illumination, CIE [*McKinlay and Diffey*, 1987]. The UV Index (UVI) is obtained by multiplying E_{er} (expressed in W m^{-2}) by 40. This index is used worldwide to inform about the risk of overexposure to UV radiation [*Vanicek et al.*, 2000]. UVI values are predicted using various radiative transfer models of different complexity, which yield results of different quality [*Koepke et al.*, 1998]. Because of both scattering and absorption increases for shorter wavelengths and $\varepsilon\lambda$ is higher for these wavelengths, the AE is generally higher when it is referred to UVB or to erythemally weighted irradiance.

[5] Field measurements of AE have been conducted in different places and under different atmospheric conditions. The measurements are generally made using broadband and spectral radiometers with different optical characteristics, wavelength range and spectral response and few AE values are determined by simultaneous measurements. Theoretical lower limit for AE (due to 100-hPa pressure difference) decreases from 10% at 300 nm to ~5% at 330 nm at SZA 50° [*Krotkov et al.*, 1998]. Most field measurements of AE are higher than this theoretical limit, which is expected due to additional ozone and aerosol decrease with altitude. For example, the AE derived by *Blumthaler et al.* [1992] from annual totals in the Alps yields 19% km^{-1} for UVB and 11% km^{-1} for UVA. Simultaneous measurements of UV spectral irradiance showed an AE of 9% km^{-1} at 370 nm and 24% km^{-1} at 300 nm [*Blumthaler et al.*, 1994]. Lower AE at 380 nm was reported by *Cabrera et al.* [1995] in Chile: 4% km^{-1} for clean air conditions and 8% km^{-1} for polluted conditions. *Piazena* [1996] measured an increase of about 8–10% km^{-1} in the tropical Chilean Andes for UVB. *Dubrovský* [2000] reported UVB AE ranging 4–8% km^{-1} for measurements in the Czech Republic averaged over 10 months. *McKenzie et al.* [2001] determined the AE using measurements from Mauna Loa (Hawaii) and Lauder (New Zealand) showing a decrease in AE when both sites are under pristine air conditions as expected from theoretical models. *Zaratti et al.* [2003] found that erythemally weighted irradiance increased with altitude at an approximate rate of 7% per kilometer in a field campaign in Bolivia. Also in this country *Pfeifer et al.* [2006] measured the AE for erythemal irradiance at different altitude pairs and found values of 16–31% km^{-1} between the highest two and 5–20% km^{-1} between the lowest two. The same report showed increases in AE of 7–16% km^{-1} in Germany. A recent study by *Dahlback et al.* [2007] examining measurements in the altitude region from 3000 m to 5000 m in Lhasa (Tibet) under clear-sky and snow-free conditions indicated an AE of 7–8% km^{-1} for erythemal UV dose rates and 3% km^{-1} at a wavelength of 340 nm, which is in agreement with the theoretical limit [*Krotkov et al.*, 1998], if pressure variation with altitude is taken into account.

[6] For cloudless snow-free conditions, atmospheric turbidity is the main cause of variability in the AE due to the different absorption and scattering depending on the source and type of aerosol present. It is therefore important in AE studies to characterize the air masses in detail such as shown by *Wenny et al.* [1998].

[7] UV radiation reaches high levels in the South of Spain during late spring and summer. The small SZA together with the presence of high mountains in the Iberian Peninsula makes AE characterization important. This work aims to determine the AE from simultaneous measurements made at different altitudes up a mountain. A wide variety of instruments, previously calibrated and intercompared [*Estellés et al.*, 2006; *Díaz et al.*, 2007] were used to study the spectral and integrated variation in irradiance with altitude. The results are related to the optical properties of the aerosols at each site. Section 2 gives an overview of the VELETA-2002 campaign and section 3 describes the instruments used. Results for spectral and broadband measurements are presented and discussed in section 4 taking into account the turbidity conditions. Section 5 summarizes the conclusions.

2. Overview of the VELETA-2002 Campaign

[8] The field campaign "Evaluation of the Effects of Elevation and Aerosols on the Ultraviolet Radiation" (VELETA-2002) took place at the beginning of the summer of 2002 in the Sierra Nevada Massif, close to Granada, in the southeast of Spain.

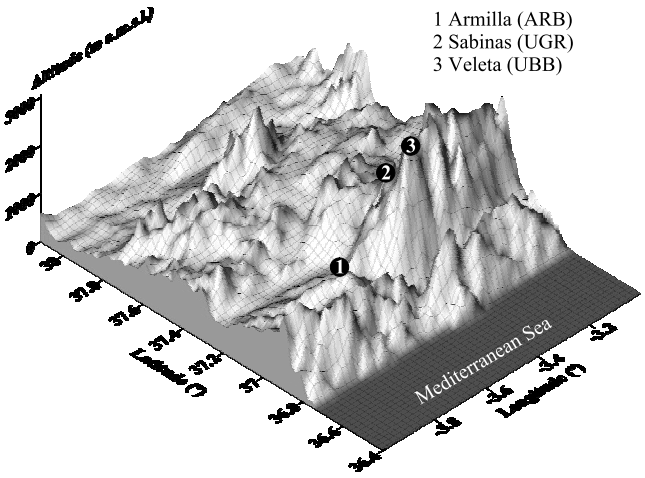

Figure 1. Locations of the three stations on the north face of the Sierra Nevada Massif considered in this study.

[9] One of the goals of the campaign was to evaluate the impact of aerosols on UV irradiance. The instruments used were positioned at various stations from sea level up to 3398 m a.s.l. An overview of the project characteristics was described by *Alados-Arboledas et al.* [2003a]. The campaign was divided into two parts: a calibration period and an observational period. During the first period, from 8 to 11 July, the instruments were calibrated (using laboratory lamps) and intercompared in order to assess the quality of the measurements. In the second period, the instruments were arranged at different altitudes and took measurements for a week (13 to 19 July). The instruments shared a data collection routine including both starting time and duration.

[10] In recent years several papers have been published concerning different aspects of the VELETA-2002 measurements. *Díaz et al.* [2007] analyzed the effects of atmospheric aerosols on spectral global UV irradiance. *Estellés et al.* [2006] intercompared spectroradiometers and Sun photometers to determine the aerosol optical depth. *Alados-Arboledas et al.* [2008] characterized the aerosol columnar properties at the two sites of the Sierra Nevada Massif. *Molero et al.* [2005] compared the aerosol size from ground-based measurements and from Lidar. *Lorente et al.* [2004] reported preliminary results of AE by analyzing two stations on one day of the campaign.

[11] The present work is a broad study of the AE at the north face of the Sierra Nevada Massif. Three observation sites were used: Armilla (680 m a.s.l.), where the previous intercomparison was carried out, Sabinas (2200 m a.s.l.) and Veleta (3398 m a.s.l.); hereafter the three stations, according to their altitude, are denoted as LOW, MED and HIGH respectively. The lowest site was greatly affected by urban aerosols [*Alados-Arboledas et al.*, 2003b; *Lyamani et al.*, 2004]. The other two sites were less affected by the pollution in the lowest tropospheric layer. Figure 1 shows the location of the stations and the complex topography of the area, represented using the GTOPO30 global digital elevation model [*U.S. Geological Survey*, 2004].

[12] The three locations are very close: north-south distances are less than 2.5 km and east-west, less than 19 km. Sabinas and Veleta are separated by less than 2 km along the x, y and z axes. The proximity of the stations makes the AE values more reliable: the sites are almost vertically aligned (i.e., most differences between observations at the different sites are probably caused by differences in altitude). All three sites can be considered part of the same atmospheric column.

[13] The influence of the mountainous relief on the UV radiation due to the horizon obstruction has been examined in LOW and MED stations and obstruction modification factors of the diffuse irradiance have been calculated. These factors were determined using a digital elevation model and considering an isotropic distribution of diffuse solar irradiance over the sky dome. The maximum elevation in LOW and MED stations is 5.7° and 12.0°, respectively, due to the obstructions of the summit to the east. Results show that measurements over horizontal surfaces are not substantially disturbed by the skyline in summer since the modification factors are 0.23% and 0.06% for MED and LOW stations, respectively. However, under snow conditions, the reflected irradiance should be considered as the modification factors could be substantially higher [*Hess and Koepke*, 2008].

3. Instruments and Calibration

[14] The station locations and the instruments used in this study, which included spectroradiometers, broadband pyranometers and sunphotometers, are summarized in Table 1. The spectroradiometers used in this work have double monochromator; the Bentham DM150 (HIGH) and the Brewer MKIII, which has a Teflon diffuser as an optical input. The Bentham instrument measured spectrally from 290 to 365 nm every 0.5 nm and from 365 to 800 nm, every 5 nm; the Brewer only measured from 290 nm up to 363 nm (also every 0.5 nm).

[15] To evaluate the relative differences among instruments all the spectroradiometers took measurements from reference lamps. Each one also took measurements from a mercury lamp in order to correct the wavelength misalignment and to obtain the slit function and the Full Width at Half Maximum value (FWHM). The wavelength shift of each instrument was determined using the technique developed by *Slaper et al.* [1995], *Slaper* [1997] and *Slaper and Koskela* [1997] on the basis of first detecting the Fraunhofer lines to align the spectral measurements. Then, the spectral irradiances measured with different spectroradiometers are deconvoluted first with the specific slit function and then smoothed with a common triangular slit function with a 1 nm FWHM. This procedure eliminates the differences in optical characteristics of the instruments and allows us to

Table 1. Description of Stations and Instruments Used in This Work

Station	Code	Latitude	Longitude	Altitude	Spectroradiometer	Broadband Pyranometer	Other Instruments
Armilla	LOW	37.13°N	3.62°W	680 m	Brewer MKIII	YES UVB1	LICOR,CIMEL, sounding station
Sabinas	MED	37.12°N	3.43°W	2200 m		YES UVB1	LICOR,CIMEL
Veleta	HIGH	37.11°N	3.41°W	3398 m	Bentham DM150	YES UVB1	LICOR

compare readings to reference standard. The reference spectroradiometer was the Brewer MKIII due to the stability of its calibration factors, and the fact that it had the smallest wavelength shift: less than 0.05 nm [*Díaz et al.*, 2007]. This instrument was part of the reference in previous campaigns such as El Arenosillo in 1999 [*Labajo et al.*, 2004]. *Díaz et al.* [2007] analyzed the spectroradiometers data from the campaign and showed that the Bentham instruments had good agreement with low deviation from the reference.

[16] Broadband pyranometers (Robertson-Berger type model YES UVB-1) took measurements continuously at each observation site. They measured voltages that were converted to erythemal irradiance by a calibration constant. This factor was determined for each pyranometer by comparison to a standard and it did not depend on the ozone content or the SZA. The UVI was calculated from the 30-min irradiance average. The YES UVB-1 pyranometers have a similar spectral response to the erythemal action spectrum, although there are some differences (especially in the UVA region). The fall of the spectral response takes place at a wavelength about 10 nm higher where the CIE action spectrum falls. Therefore, the sensitivity of the pyranometer to ozone content changes is less than the one calculated from a spectral irradiance weighted with the CIE action spectrum.

[17] Aerosol optical characteristics were determined from direct solar radiation measurements recorded with LICOR-1800 spectroradiometers and solar and sky measurements with CIMEL CE318 sunphotometers. The LICOR-1800 spectroradiometers used in this work were equipped with a Teflon diffuser that sends the light to a single monochromator with a FWHM of 6.25 nm. It can be used in the 300–1100 nm range with a wavelength step of 1 nm, although the shortest wavelengths in the UVB range have great uncertainties. The instrument measures global spectral irradiance but it can measure direct irradiance using a collimator with a field of view around 5° and a construction based on the design previously developed at the U.S. Solar Energy Research Institute [*Cannon*, 1986]. *Martínez-Lozano et al.* [2003] have determined the uncertainty of these direct irradiance measurements in 5%. During the first week, the LICOR-1800s were calibrated with reference lamps provided by the manufacturer and using the Langley method as described by *Estellés et al.* [2006]. *Estellés et al.* [2006] showed that after common calibration the deviation between these instruments and the CIMEL CE318 sunphotometer was 0.01 for AOD. This aerosol parameter varies with the wavelength; so the AOD derived from LICOR measurements at 380 (UVA), 440 and 500 nm (in the visible band, typically used to characterize aerosols) have been used in this study.

[18] During the campaign a radiosonde and an ozonesonde were launched daily from LOW station. Upper air data provided a vertical description of atmospheric variables such as temperature, humidity, water vapor content, and ozone concentration.

4. Results and Discussion

4.1. Turbidity Conditions

[19] During the campaign there were two clearly differentiated air masses associated to two synoptic situations: a polar maritime air mass and a tropical continental air mass (Saharan dust event). The first one was the result of a strong high-pressure system located over the Azores and a low in the Mediterranean Sea. It entailed weak N–NE winds both at surface and at higher layers in Southern Spain. From 17 July the situation changed. A deep low-pressure area advancing from the Atlantic Ocean displaced the anticyclone northward. Simultaneously, a thermal low formed over the Iberian Peninsula with a weak isobaric gradient. The winds turned to S–SE.

[20] The different source of the air masses led to differences in the type and characteristics of the aerosols. The 5-day backward trajectories determined using the NOAA HYSPLIT model (R. R. Draxler and G. D. Rolph, HYSPLIT (HYbrid Single-Particle Lagrangian Integrated Trajectory), 2003, http://www.arl.noaa.gov/ready/hysplit4.html) confirmed the two synoptic situations with the two distinct air masses. Two characteristic days of each situation were 16 and 18 July, respectively. Figure 2 shows the 120-h backward trajectories for both days at the three altitudes of the observation sites. In the first case, the polar air mass crossed source regions of anthropogenic aerosols such as oil refineries. This affected the lowest location most since the trajectory at this level is always located in the lower layers of the troposphere. This caused greater differences in turbidity among the stations. During the Saharan dust outbreak lofted aerosol layers were detected in the free troposphere [*Molero et al.*, 2005].

[21] The diurnal evolution of AOD during the second stage of the campaign at each station for each wavelength is shown in Figure 3. As expected, the highest AOD values were measured in LOW station. The high levels of anthropogenic aerosol increased the AOD value in the urban environment of the lower station whereas variations in AOD at the two higher stations were not noticeable since they were less influenced by the urban turbidity [*Alados-Arboledas et al.*, 2008]. It is also evident (Figure 3) that on the first and last days (13 and 18 July) the values were higher than on the other days of the campaign. On the first day the synoptic situation favored the long-range transport of aerosols of air masses coming from the Easter coast of North America. This area was affected by large smoke plumes from Canadian forest fires as MODIS images indicated [*Alados-Arboledas et al.*, 2008]. On the last day, an intrusion of mineral dust was responsible for the increase in AOD. This kind of event is characterized by an increased presence of larger particles, usually located in lofted layers in the free troposphere [*Guerrero-Rascado et al.*, 2008] as shown by the variations in other aerosol properties such as the Angström exponent α and the single scattering albedo ω_0 [*Alados-Arboledas et al.*, 2008]. Lidar analysis also confirmed the Saharan source of the aerosols [*Molero et al.*, 2005].

[22] The AOD also showed daily variations with different behavior depending on the location. Those variations were related to the evolution of tropospheric turbidity throughout the day. At LOW station the aerosol amount increased in the morning to a maximum value before the noon and then decreased in the evening probably owing to the influence of traffic pollution, while at the MED station the variation was quite different. *Alados-Arboledas et al.* [2004, 2008] examined daily variation in different optical properties of aero-

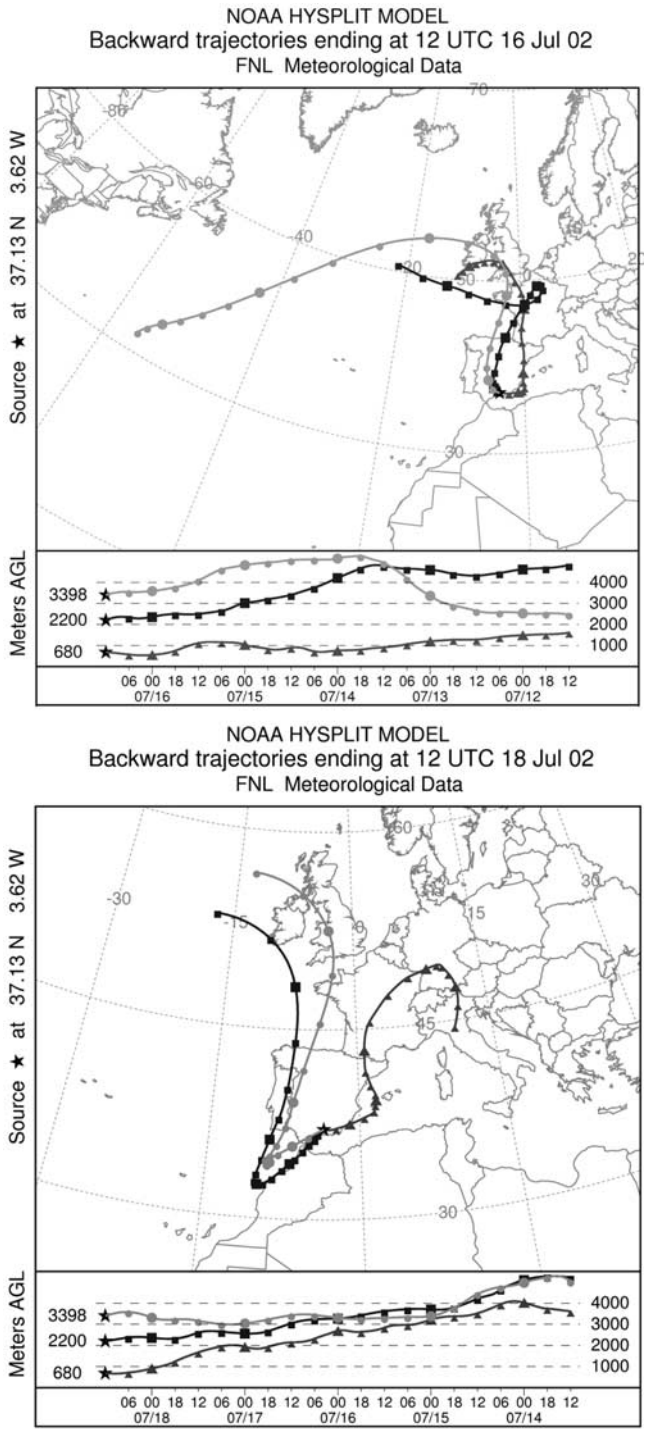

Figure 2. Backward trajectories for two characteristic days in the campaign: (top) 16 July (maritime air mass) and (bottom) 18 July (continental air mass associated to a Saharan dust event).

sols measured at this observation site. During the morning, MED was in the free troposphere and the AOD was low. The growth of the planetary boundary layer (PBL) through the day gave rise to an increase in turbidity. In the afternoon, the site was inside the PBL and the AOD reached values comparable with those measured at LOW. At the highest

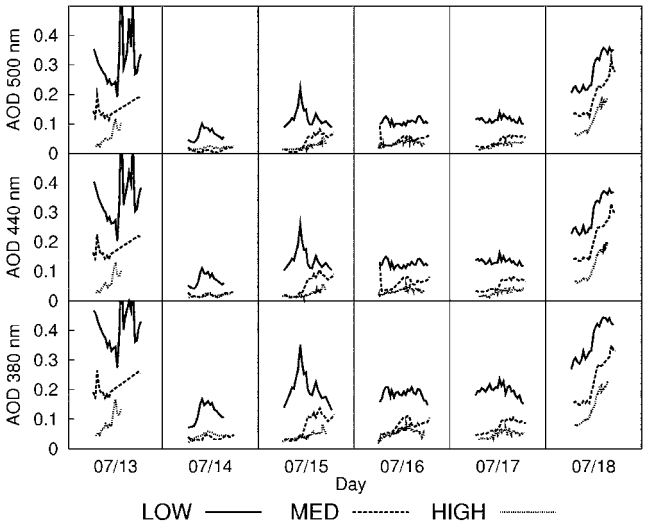

Figure 3. Evolution of aerosol optical depth (AOD) at the three different stations considered in this study at 380, 440 and 500 nm. Note the contrast between 14 July, corresponding to a polar maritime air mass, and 17 July when the Saharan dust intrusion started.

location, AOD showed similar daily patterns but less pronounced.

4.2. AE From Spectral Measurements and Simulations

[23] Figure 4 shows an example of concurrent spectral measurements at LOW and HIGH stations. Higher irradiance values found at HIGH station are due to less Rayleigh scattering (due to pressure difference between the two stations) and also by less aerosol absorption and scattering due to cleaner air. At wavelengths shorter than 320 nm, tropospheric ozone also is a factor to be considered. During summer, when surface UV radiation is high, photochemical reactions produce tropospheric ozone from NO_x compounds originated by urban and industrial sources. Moreover, ozone concentration profile will influence AE when one of sites is

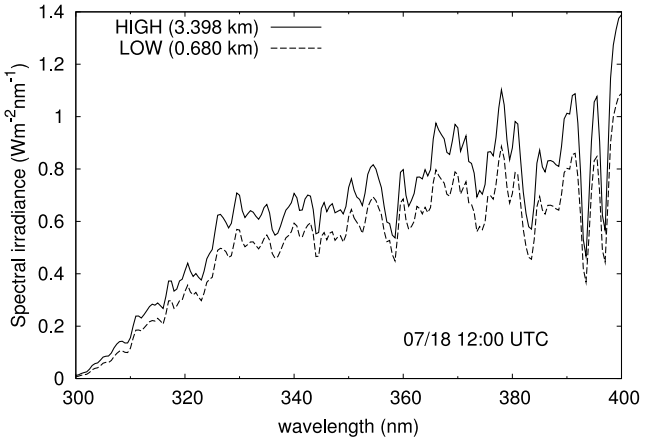

Figure 4. Example of concurrent spectral irradiance measurements recorded at LOW and HIGH stations corresponding to 18 July 2002, 1200 UTC, when high values of atmospheric turbidity associated with the Saharan dust intrusion were observed.

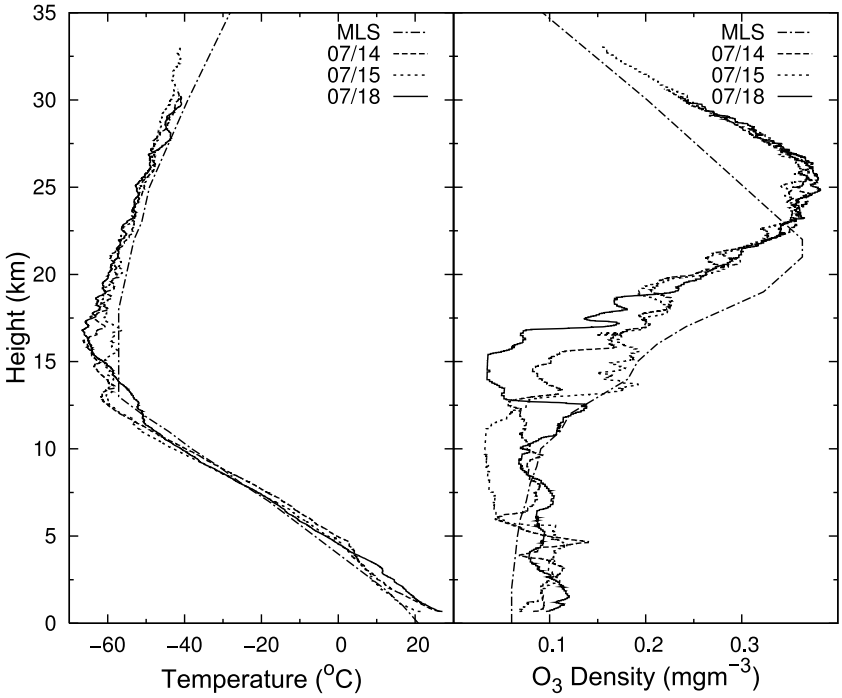

Figure 5. Observed vertical profiles of temperature and ozone density measured on 14, 15, and 18 July and the midlatitude summer (MLS) reference profiles used in the SBDART 2.4 radiative transfer model.

highly influenced by air pollution as is the case for LOW affected by heavy traffic.

[24] The total ozone column at LOW was determined from the Brewer MKIII spectroradiometer measurements whereas for the other sites was calculated by correcting the Brewer measurements for the reduction in ozone with altitude. Furthermore, the ozonesondes launched from LOW once a day during the campaign allowed us to determine the total ozone column above the three altitudes. The vertical ozone decay during the campaign varied from 4.0 ± 0.3 DU km^{-1} to 5.4 ± 0.5 DU km^{-1}. It should be noted that these values differ from the 3 DU km^{-1} characteristic of a midlatitude summer (MLS) atmospheric profile as considered in the radiative transfer model SBDART 2.4 [*Ricchiazzi et al.*, 1998], which is used later. This is illustrated by Figure 5 which shows the MLS temperature and ozone density profiles and actual profiles observed during the campaign. Though the MLS temperature profile is similar to observed profiles, the ozone density indicated by MLS reference is lower than observations below 5 km.

[25] To assess the influence of tropospheric ozone and Rayleigh scattering on spectral AE the radiative transfer model SBDART model version 2.4 has been used. A clean atmosphere, without aerosols, has been considered in the SBDART simulations. Different simulations have been run, considering both a standard MLS ozone profile, as mentioned earlier with 3 DU km^{-1}, and also observed ozone profiles with 3, 4 and 5 DU km^{-1}, respectively. In all cases, the total ozone column used for LOW station was obtained from the Brewer spectroradiometer records. Figure 6 shows the UVI AE between LOW and HIGH stations produced by tropospheric ozone as a function of SZA for a day of the campaign (16 July). The use of a standard MLS ozone profile causes an underestimation of the AE of about 1% km^{-1} compared to using a real profile with an ozone decay of 5 DU km^{-1}. Moreover, it should be noted that for SZA < 60° the UV AE increases with SZA owing to the influence of the relative air mass. However, for SZA >60° most part of UV solar radiation is diffuse and as a consequence, the AE diminishes as SZA increases. As shown in Table 2, the AE due to ozone did not change substantially during the campaign, as expected by the little variations recorded in the total ozone column during the observing period.

[26] Figure 7 shows the observed spectral AE (LOW-HIGH) at 12 UTC for two days: a clear day with few aerosols (16 July) and a day affected by a Saharan dust event (18 July). The spectral range corresponds to the Brewer spectroradiometer wavelength interval. Aerosols influence the spectral AE owing to their effect on spectral irradiance. On the clear day, AE varied from 20 to 8% km^{-1} spectrally. The UVB region was characterized by a strong decrease with increasing wavelength. At 300 nm, AE was about twice as much as at 320 nm in agreement with theoretical calculation [*Krotkov et al.*, 1998]. However, the values in the UVA range were fairly constant. During the Saharan dust episode, the increase at short wavelengths was slightly more pronounced because of sharp increase in dust absorption at UVB wavelengths. Since dust has less absorption in the UVA and visible wavelengths, the AE increase in the UVA wavelengths was smaller, so the differences between UVB and UVA were greater in this case. During 16 July, the spectral AE at 300 nm varied from 20% km^{-1} to 35% km^{-1} for LOW-HIGH. The lowest AE values were recorded at noon while higher values were determined for larger solar zenith angles (early morning and late afternoon). It should be noted that the difference of AE between the two days is nearly constant and independent of the wavelength.

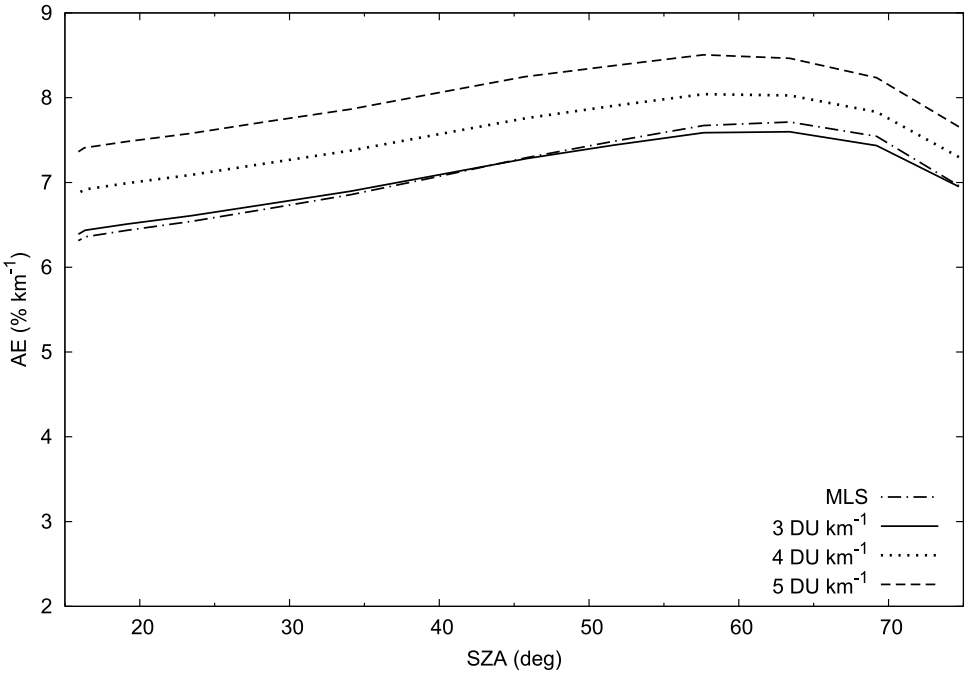

Figure 6. Simulated altitude effect (AE) between LOW and HIGH stations produced by tropospheric ozone for 16 July considering four possible ozone vertical profiles: MLS and ozonesonde measurement with tropospheric ozone decay: 3, 4, and 5 DU km^{-1}. The radiative transfer model used was SBDART 2.4.

[27] Table 2 shows the AE due to ozone and aerosols at 1200 UTC for the 2 days discussed above. These values were derived from SBDART simulations assuming the optical properties retrieved from measurements, which allowed estimating the effect due to aerosol absorption and scattering. Interestingly, the aerosol AE nearly doubled during the Saharan air intrusion event (18 July) compared to the much cleaner, pristine atmosphere, only two days before (16 July). *Alados-Arboledas et al.* [2008] provides a detailed description of the increase and change of optical aerosol properties during that event. There are also other factors to be considered such as absorption due to atmospheric gases associated to the heavy traffic and urban activity in the LOW station. As commented previously for the ozone column, at high SZA, the aerosol contribution to AE is more important and for example, even for a clear atmosphere, this effect would predominate compared to a low SZA during a Saharan dust event.

[28] Table 3 shows the AE between the LOW and HIGH stations computed at noon for UVB, UVA bands and for UV index. The observed AE ranges were 7–11% km^{-1} for UVB, 6–8% km^{-1} for UVA and 11–14% km^{-1} for UVI. It can be noted the AE increase for shorter wavelengths and the high values for the erythemally weighted irradiance. A remarkable contrast is found between the 16 July pristine day and the Saharan dust event on 18 July when the highest values of AE for UVI were reached.

Table 2. Simulated Altitude Effect at Noon for 16 and 18 July Between LOW and HIGH Stations Showing Contributions for Ozone Absorption and Aerosols Using the SBDART 2.4 Model[a]

Wavelength (nm)	Ozone Absorption		Aerosols	
	16 July	18 July	16 July	18 July
300	9.6	10.0	1.9	3.6
310	2.5	2.6	1.5	2.8
320	0.8	0.9	1.4	2.5
330	0.0	0.0	1.1	2.2

[a]SZA is equal to 16°. Altitude effect is expressed in % km^{-1}.

4.3. AE From Broadband Measurements

[29] Figure 8 shows the variation of the UV index measured with broadband pyranometers at the three selected

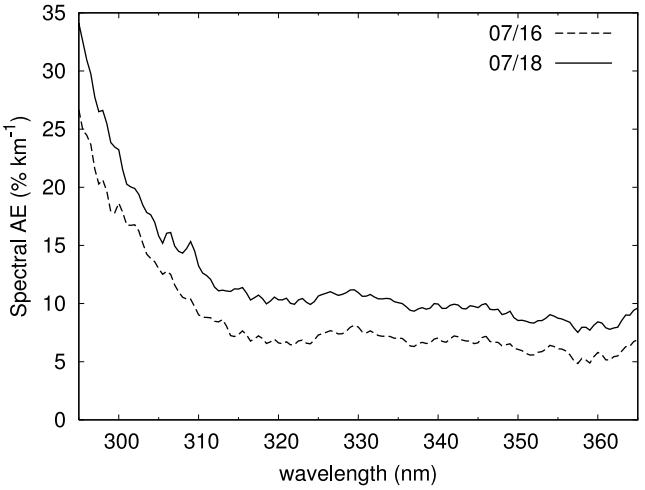

Figure 7. Variation in observed AE with wavelength at 1200 UTC during the Saharan dust event (18 July) and on a clear day (16 July). A strong wavelength dependence is observed in the UVB band, more intense for the day with higher turbidity (18 July).

Table 3. Observed Altitude Effect at Noon Between LOW and HIGH Stations Determined From Spectroradiometer Measurements for UVB, UVA, and UVI[a]

	AE (LOW-HIGH) (% km^{-1})		
Day	UVB	UVA	UVI
14 July	9.4	5.9	11.4
15 July	10.5	7.2	13.1
16 July	9.0	6.8	11.7
17 July	10.6	6.8	13.4
18 July	11.0	8.3	13.9

[a]SZA is equal to 16°.

locations throughout 16 July. The effect of altitude on UVI is evident, reaching at noon almost three units between the LOW and HIGH stations. Table 4 shows the AE from broadband measurements at noon for the three stations. During the northern air mass situation, the AE on UVI was generally close to 10% km^{-1} for LOW-HIGH and MED-HIGH and somewhat lower in the LOW-MED. At the end of the campaign, with the intrusion of mineral aerosols, there was a consequent increase in AE. This increase was more evident when HIGH was the top station.

[30] The daily variability of AE depends on the two stations considered as shown in Figure 9. If it is calculated with the lowest and the highest stations, it is quite constant during the northern air mass period. It only shows different behavior at the end of the campaign owing to changes in atmospheric aerosols. The values range from 10% km^{-1} to 15% km^{-1} for UVI, which are higher than the AE of 8% km^{-1} used as an average value by COST-713 Action [*Vanicek et al.*, 2000]. The larger daily variability is shown in the LOW-MED case. As mentioned before, there was a diurnal increase in AOD at MED due to the growth of the PBL through the day. In the morning, when this site is representative of free troposphere, a higher AE with regard to LOW is observed. This AE decreases during the day and reaches lower values in the afternoon since the differences in AOD are smaller. HIGH is much less influenced by the vertical development of the PBL. Early in the morning, MED and HIGH are considered representative of the free troposphere. So the AE value is very low since the role of Rayleigh scattering is much more important than that of aerosols. As the PBL grows, the difference in AOD between the locations increases, with the consequent increase in AE.

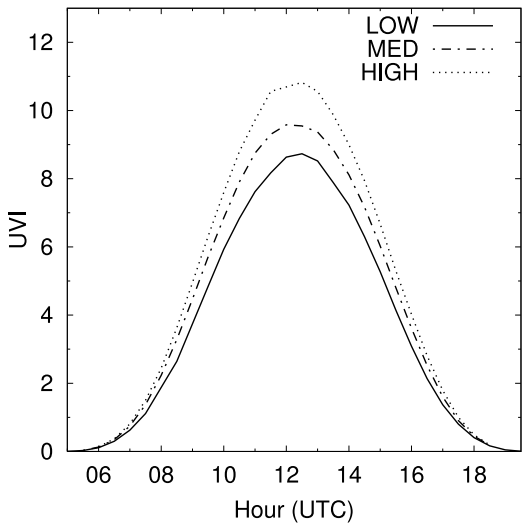

Figure 8. Evolution of UVI at LOW, MED, and HIGH determined from broadband measurements during 16 July. Note the maximum value of 11 observed at HIGH (Veleta peak, 3398 m a.s.l.) corresponding to a category of "Extreme" according to the COST-713 classification [*Vanicek et al.*, 2000].

[31] In accordance with the results, AE is not linearly dependent on SZA since the growth of PBL introduces differences throughout the day. Figure 10 shows the variation of AE with SZA for a typical day during the northern air mass situation. In this case, averages of morning and afternoon measurements have not been calculated to avoid filtering possible differences throughout the day due to the growth of the PBL. AE is represented by broadband measurements and by erythemally weighted irradiance for LOW-HIGH case. The values for pyranometers are close to the tendency in the UVB range, especially for low SZA. In this case, the differences in turbidity remain fairly constant throughout the day. For this reason the morning-afternoon differences are not significant. However, if the MED site is considered, then AE variations with SZA are more important. For LOW-MED, AE decreases almost linearly with SZA in the morning. Then it shows the opposite tendency in the afternoon when it is located inside the mixing layer. For the case of the two high stations, AE differences throughout the day are less important as aerosol load remained similar over both sites.

[32] The UVI AE values obtained with broadband pyranometers for the LOW-HIGH case are similar to those estimated with spectroradiometers following an identical qualitative evolution during the period considered. However, broadband derived AE values underestimate spectral ones by 2–3% km^{-1} (absolute difference) at noon as also seen in Figure 10. The differences in AE determined from broadband and erythemally weighted spectroradiometer measurements could be related to the different spectral and angular responses of each broadband pyranometer. On one hand, the spectral response of each pyranometer can differ from the CIE action spectrum. On the other hand, according to an intercomparison of this kind of instruments carried out at PMOD/WRC in Davos (Switzerland) [*Gröbner et al.*, 2007; *Hülsen et al.*, 2008], the particular angular response of the YES pyranometers can introduce cosine corrections from 14% to 25%. Despite the effect of the obstruction corrections is small, the angular response of each individual pyranometer can also represent differences in the cosine

Table 4. UVI Altitude Effect at 1200 UTC From Broadband Measurements

	AE (% km^{-1})		
Day	LOW-HIGH	LOW-MED	MED-HIGH
14 July	8.6		
15 July	10.9	10.6	9.8
16 July	9.4	7.6	10.4
17 July	10.4	9.3	10.3
18 July	12.0	9.9	12.7

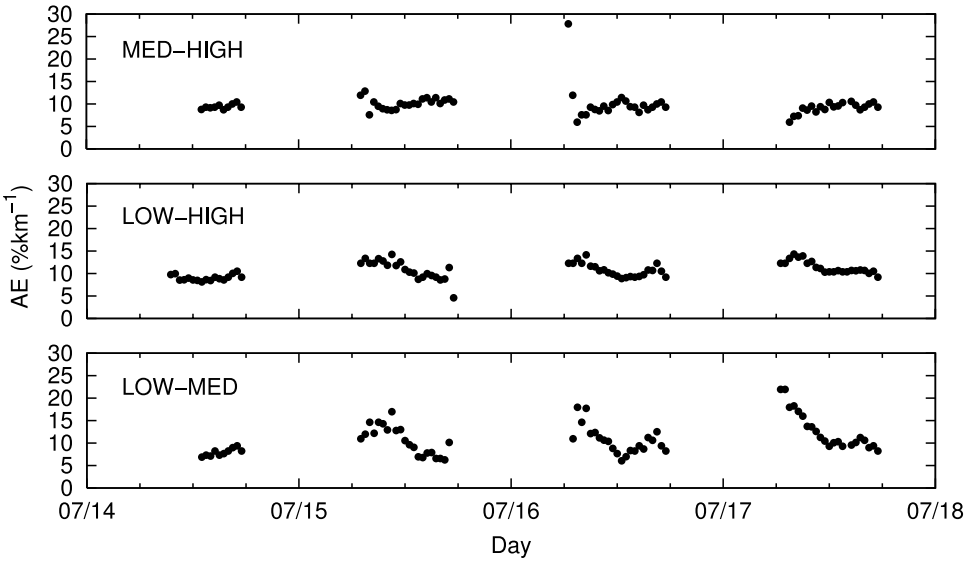

Figure 9. Diurnal evolution of AE as determined from broadband measurements between the central days of the campaign.

correction (between 0.4% and 0.8% in the PMOD/WRC intercomparison campaign).

5. Summary and Conclusions

[33] The VELETA-2002 campaign studied UV irradiance examining in detail the effect of aerosols and altitude. The campaign started with a calibration period and a 1-week observing period. The observing period of the campaign was characterized by a maritime polar air mass with low AOD and ended with a tropical continental air mass (Saharan dust event). The aerosols from first period were mainly from anthropogenic sources and were incorporated to the air mass as it passed over the Iberian Peninsula. During the last days, the situation changed abruptly when the intrusion of Saharan dust took place at all levels with a rapid increase of aerosol concentration.

[34] Results from simultaneous measurements of spectral and broadband UV irradiances confirm the main features of the UV altitude effect: an increase for shorter wavelengths (i.e., increasing from UVA, UVB to erythemally weighted irradiances) and with atmospheric turbidity. The tropospheric ozone profile is another cause of AE variability. From the results of AE simulations carried out by means of the SBDART radiative transfer model, one observes that the use of a standard MLS ozone profile caused an underestimation of the AE of about 1% km^{-1} compared to that computed using a real profile with an ozone decay of 5 DU km^{-1}.

[35] The dependence of AE on solar zenith angle was more difficult to evaluate because of the daily rise of the PBL air in the afternoon. However, an AE increase with SZA was generally observed when turbidity conditions experimented

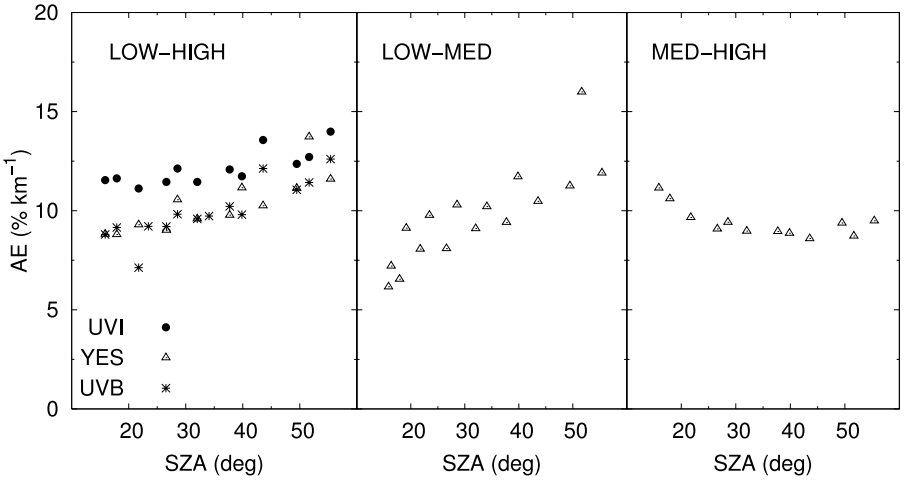

Figure 10. Dependence of AE on SZA for the three stations. AE is determined from broadband measurements (YES) and from CIE-weighted spectral irradiance (UVI) and integrated over the UVB region (UVB) for the LOW-HIGH case.

little variations. At noon (SZA equal to 16°), UVA AE was 6–8% km^{-1} and it increased to 7–11% km^{-1} for UVB and 11–14% km^{-1} for UVI.

[36] The maximum AE values were reached for UVB and UVI during the Saharan dust event. The AE determined from broadband pyranometers with erythemal response agreed qualitatively well but was lower than AE derived from spectral measurements by 2–3% km^{-1}. These differences could be explained by the particular spectral and angular response of each individual pyranometer. When the atmosphere at two sites is clear, the measured AE was close to the lower theoretical limit for Rayleigh atmosphere (~5% km^{-1} at 330 nm [*Krotkov et al.*, 1998]) but it is quite different when the locations are highly influenced by aerosols. According to these results, it is suggested to consider AE factors higher than 8% km^{-1} (used as an average value by the European research action COST-713) when a polluted lower station and a higher station with less pollution are being compared. In order to achieve a better evaluation of the AE by radiative transfer models an adequate characterization of the optical properties and the source of the atmospheric aerosols are necessary.

[37] **Acknowledgments.** This work was supported by the Spanish Ministry of Education and Science through coordinated projects REN2000-0903-C08/CLI and CGL2005-03428-C04-04. The authors gratefully acknowledge the NOAA Air Resources Laboratory (ARL) for the provision of the HYSPLIT transport and dispersion model and READY website (http://www.arl.noaa.gov/ready.html) used in this publication.

References

Alados-Arboledas, L., et al. (2003a), VELETA 2002 field campaign, *Geophys. Res. Abstr.*, *5*, 12,218.

Alados-Arboledas, L., H. Lyamani, and F. J. Olmo (2003b), Aerosol size properties at Armilla, Granada (Spain), *Q.J.R. Meteorol. Soc.*, *129*(590), 1395–1413, doi:10.1256/qj.01.207.

Alados-Arboledas, L., et al. (2004), Atmospheric aerosol changes in the vertical followed by sunphotometers and telephotometers during VELETA 2002, *J. Aerosol Sci.*, *35*(S1), 503–504, doi:10.1016/j.jaerosci.2004.06.039.

Alados-Arboledas, L., et al. (2008), Aerosol columnar properties retrieved from CIMEL radiometers during Veleta 2002, *Atmos. Environ.*, *42*, 2654–2667, doi:10.1016/j.atmosenv.2007.10.006.

Bais, A., et al. (2007), Surface ultraviolet radiation: Past, present and future, *Rep. 50*, chap. 7, pp. 7.1–7.54, Global Ozone Res. Monit. Proj., World Meteorol. Org., Geneva.

Blumthaler, M., W. Ambach, and W. Rehwald (1992), Solar UV-A and UV-B radiation fluxes at two alpine stations at different altitudes, *Theor. Appl. Climatol.*, *46*, 39–44, doi:10.1007/BF00866446.

Blumthaler, M., A. R. Webb, G. Seckmeyer, A. F. Bais, M. Huber, and B. Mayer (1994), Simultaneous spectroradiometry: A study of solar UV irradiance at two altitudes, *Geophys. Res. Lett.*, *21*, 2805–2808, doi:10.1029/94GL02786.

Blumthaler, M., W. Ambach, and R. Ellinger (1997), Increase in the UV radiation with altitude, *J. Photochem. Photobiol. B*, *39*, 130–134.

Cabrera, S., S. Bozzo, and H. Fuenzalida (1995), Variations in UV radiation in Chile, *J. Photochem. Photobiol. B*, *28*, 137–142.

Cannon, T. W. (1986), Spectral solar irradiance instrumentation and measurements techniques, *Solar Cells*, *18*, 233–234.

Dahlback, A., N. Gelsor, J. J. Stamnes, and Y. Gjessing (2007), UV measurements in the 3000–5000 m altitude region in Tibet, *J. Geophys. Res.*, *112*, D09308, doi:10.1029/2006JD007700.

Díaz, A. M., et al. (2007), Aerosol radiative forcing efficiency in the UV region over Southern Mediterranean: VELETA2002 campaign, *J. Geophys. Res.*, *112*, D06213, doi:10.1029/2006JD007348.

Dubrovský, M. (2000), Analysis of UV-B irradiances measured simultaneously at two stations in the Czech Republic, *J. Geophys. Res.*, *105*, 4907–4913, doi:10.1029/1999JD900374.

Estellés, V., et al. (2006), Intercomparison of spectroradiometers and Sun photometers for the determination of the aerosol optical depth during the VELETA-2002 field campaign, *J. Geophys. Res.*, *111*, D17207, doi:10.1029/2005JD006047.

Farman, J. C., B. G. Gardiner, and J. D. Shanklin (1985), Large losses of total ozone in Antarctica reveal seasonal ClO_x/NO_x interaction, *Nature*, *315*, 207–210, doi:10.1038/315207a0.

Gröbner, J., G. Hülsen, L. Vuilleumier, M. Blumthaler, J. M. Vilaplana, D. Walker, and J. E. Gil (2007), Report of the PMOD/WRC-COST calibration and intercomparison of erythemal radiometers, report, Phys. Meteorol. Obs., Davos, Switzerland. (Available at http://www.pmodwrc.ch/euvc/pdf/ReportCOST726.pdf)

Guerrero-Rascado, J. L., B. Ruiz, and L. Alados-Arboledas (2008), Multispectral lidar characterization of the vertical structure of Saharan dust aerosol over southern Spain, *Atmos. Environ.*, *42*, 2668–2681.

Hess, M., and P. Koepke (2008), Modelling UV irradiances on arbitrarily oriented surfaces: Effects of sky obstructions, *Atmos. Chem. Phys.*, *8*, 3583–3591.

Hülsen, G., J. Gröbner, A. Bais, M. Blumthaler, P. Disterhoft, B. Johnsen, K. O. Lantz, C. Meleti, J. M. Vilaplana Guerrero, and L. Ylianttila (2008), Intercomparison of erythemal broadband radiometers calibrated by seven UV calibration centers in Europe and the USA, *Atmos. Chem. Phys.*, *8*, 4865–4875.

Koepke, P., et al. (1998), Comparison of models used for UV Index calculations, *Photochem. Photobiol.*, *67*(6), 657–662, doi:10.1111/j.1751-1097.1998.tb09109.x.

Krotkov, N. A., P. K. Bhartia, J. R. Herman, V. Fioletov, and J. Kerr (1998), Satellite estimation of spectral surface UV irradiance in the presence of tropospheric aerosols: 1. Cloud-free case, *J. Geophys. Res.*, *103*, 8779–8793, doi:10.1029/98JD00233.

Krotkov, N. A., P. K. Bhartia, J. Herman, J. Slusser, G. Scott, G. Labow, A. P. Vasilkov, T. F. Eck, O. Dubovik, and B. N. Holben (2005), Aerosol UV absorption experiment (2002 to 2004), 2. Absorption optical thickness, refractive index, and single scattering albedo, *Opt. Eng.*, *44*(4), 041005, doi:10.1117/1.1886819.

Labajo, A., E. Cuevas, and B. de la Morena (2004), *The first Iberian UV-Visible instruments intercomparison: Final report*, report, 114 pp., Inst. Nac. de Meteorol., Madrid.

Lorente, J., et al. (2004), Altitude effect on UV Index deduced from the VELETA-2002 experimental campaign (Spain), in *Proceedings of the International Radiation Symposium*, pp. 75–78, A. Deepak, Hampton, Va.

Lyamani, H., F. J. Olmo, and L. Alados-Arboledas (2004), Long term changes in aerosol radiative properties at Armilla, Granada (Spain), *Atmos. Environ.*, *38*, 5935–5943, doi:10.1016/j.atmosenv.2004.07.021.

Martínez-Lozano, J. A., et al. (2003), Intercomparison of spectroradiometers for global and direct solar irradiance in the visible range, *J. Atmos. Oceanic Technol.*, *20*, 997–1010, doi:10.1175/1457.1.

McKenzie, R. L., P. Johnston, D. Smale, B. A. Bodhaine, and S. Madronich (2001), Altitude effects on UV spectral irradiance deduced from measurements at Lauder, New Zealand, and at Mauna Loa Observatory, Hawaii, *J. Geophys. Res.*, *106*, 22,845–22,860.

McKinlay, A., and B. Diffey (1987), A reference spectrum for ultraviolet induced erythema in human skin, *CIE J.*, *6*, 17–22.

Molero, F., et al. (2005), Comparison of aerosol size distributions measured at ground level and calculated from inversion of solar radiances, in *Remote Sensing of Clouds and the Atmosphere*, edited by K. Schäfer et al., *Proc. SPIE*, *5979*, 59790O, doi:10.1117/12.626993.

Pfeifer, M. T., P. Koepke, and J. Reuder (2006), Effects of altitude and aerosol on UV radiation, *J. Geophys. Res.*, *111*, D01203, doi:10.1029/2005JD006444.

Piazena, H. (1996), The altitude effect upon solar UV-B and UV-A irradiance in the tropical Chilean Andes, *Sol. Energy*, *57*, 133–140, doi:10.1016/S0038-092X(96)00049-7.

Ricchiazzi, P., S. Yang, C. Gautier, and D. Sowle (1998), SBDART: A research and teaching software tool for plane-parallel radiative transfer in the Earth's atmosphere, *Bull. Am. Meteorol. Soc.*, *79*(10), 2101–2114, doi:10.1175/1520-0477(1998)079<2101:SARATS>2.0.CO;2.

Slaper, H. (1997), Methods for intercomparing instruments, in *Advances in Solar Ultraviolet Spectroradiometry*, edited by A. R. Webb, *Air Pollut. Res. Rep. 63*, pp. 153–164, Off. of the Off. Publ. for the Eur. Comm., Brussels.

Slaper, H., and T. Koskela (1997), Methodology of intercomparing spectral sky measurements, correcting for wavelength shifts, slit function differences and defining a spectral reference, in *The Nordic Intercomparison of Ultraviolet and Total Ozone Instruments at Izana, October 1996: Final Report, Meteorol. Publ.*, vol. 36, edited by B. Kjeldstad, B. Johnsson, and T. Koskela, pp. 161–172, Finn. Meteorol. Inst., Helsinki.

Slaper, H., H. A. J. M. Reinen, M. Blumthaler, M. Huber, and F. Kuik (1995), Comparing ground-level spectrally resolved solar UV measurements using various instruments: A technique resolving effects of wavelength shift and slit width, *Geophys. Res. Lett.*, *22*, 2721–2724, doi:10.1029/95GL02824.

U.S. Geological Survey (2004), GTOPO30, a global digital elevation model (DEM), http://edcdaac.usgs.gov/gtopo30/gtopo30.asp, Boulder, Colo.

Vanicek, K., T. Frei, Z. Litynska, and A. Schmalwieser (2000), UV-Index for the public. *COST-713 Action*, 27 pp., Eur. Comm., Brussels.

Wenny, B. N., J. S. Schafer, J. J. DeLuisi, V. K. Saxena, W. F. Barnard, L. V. Petropavlovskikh, and A. J. Vergamini (1998), A study of regional aerosol radiative properties and effects on ultraviolet-B radiation, *J. Geophys. Res.*, *103*, 17,083–17,097, doi:10.1029/98JD01481.

Wetzel, M. A., and J. R. Slusser (2005), Mesoscale distributions of ultraviolet spectral irradiance, actinic flux, and photolysis rates derived from multispectral satellite data and radiative transfer models, *Opt. Eng.*, *44*(4), 041006, doi:10.1117/1.1889467.

Zaratti, F., R. N. Forno, J. García Fuentes, and M. F. Andrade (2003), Erythemally weighted UV variations at two high-altitude locations, *J. Geophys. Res.*, *108*(D9), 4263, doi:10.1029/2001JD000918.

L. Alados-Arboledas and F. J. Olmo, Departamento de Física Aplicada, Facultad de Ciencias, Universidad de Granada, E-18071 Granada, Spain. (alados@ugr.es; fjolmo@ugr.es)

J. Badosa, Grup de Física Ambiental, Departamento de Física, Escola Politècnica Superior, Universitat de Girona, Campus Montilivi, Politècnica II, 116B, E-17071 Girona, Spain. (jordi.badosa@udg.edu)

J. Bech, E. Campmany, X. de Cabo, J. Lorente, A. Redaño, and Y. Sola, Departament d'Astronomia i Meteorologia, Universitat de Barcelona, c/Marti i Franqués, 1, E-08028 Barcelona, Spain. (jbech@meteocat.com; ecampmany@gmail.com; xdacabo@xtec.cat; jeroni@am.ub.es; angel@am.ub.es; ysola@am.ub.es)

V. Cachorro and M. Sorribas, Grupo de Óptica Atmosférica, Facultad de Ciencias, Universidad de Valladolid, Prado de la Magdalena, S/N, E-47071 Valladolid, Spain. (chiqui@goa.uva.es; sorribasmm@inta.es)

J. P. Díaz and F. J. Expósito, Departamento de Física, Facultad de Ciencias, Universidad de La Laguna, Campus de Anchieta, Avenida Astrofisico Frandisco Sánchez, S/N, E-38206 La Laguna, Spain. (jpdiaz@ull.es; fexposit@ull.es)

A. Labajo, Agencia Estatal de Meteorología, Leonardo Prieto Castro, 8, E-28040 Madrid, Spain. (alabajo@inm.es)

J. A. Martínez-Lozano and M. P. Utrillas, Grupo de Radiación Solar, Departamento Física de la Tierra i Termodinámica, Facultat de Física, Universitat de València, c/o Dr. Moliner, 50, E-46100 Burjassot, Spain. (Jose.A.Martinez@uv.es; utrillas@uv.es)

A. M. Silva, Centro de Geofisica de Évora, University of Évora, P-7000 Evora, Portugal. (asilva@uevora.pt)

J. M. Vilaplana, Departamento de Observación de la Tierra, Teledetección y Atmósfera, Estación de Sondeos Atmosféricos de El Arenosillo, Instituto Nacional de Téecnica Aeroespacial, Ctra. San Juan del Puerto-Matalascañas Km33, E-21130 Mazagón, Huelva, Spain. (vilaplanagjm@inta.es)